Simultaneous Optimal Estimation of Mode Transition Times and Parameters Applied to Simple Traction Models

Lauren M. Miller, *Student Member, IEEE,* and Todd D. Murphey, *Member, IEEE,*

***Abstract*—An optimization-based estimation method is presented for determining mode transition times and model parameters for hybrid systems. First- and second-order optimality conditions are derived, including cross-derivative terms between transition times and parameters. Second-order optimization methods are shown to provide superior convergence to correct values in simulation, and to values within expected ranges experimentally for traction estimation of a skid-steered vehicle.**

***Index Terms*—calibration and identification, switched systems, second-order optimization.**

I. Introduction

MANY systems in robotics experience discrete transitions between distinct dynamic modes and depend on potentially uncertain parameters. A method for robustly estimating when transitions between modes in hybrid systems occur, based on potentially coarse data, is necessary due to modeling and parametric uncertainty in real-world systems. Operation in unknown environments presents the additional need for terrain parameter identification. This paper focuses on efficient estimation of mode transition times and parameter values using hybrid optimization techniques for nonlinear, time-varying systems. It will be shown that these two problems are nontrivially coupled.

The contribution of this paper is a simplified derivation of the second order optimality conditions for optimization-based simultaneous transition time and parameter estimation for hybrid systems, which is extended to the cross-derivative terms in the Hessian; this estimation method is validated experimentally and in simulation, and estimation performance is shown to degrade gracefully as a function of measurement variance.

The least-squares optimization method presented relies on calculation of the gradient and the Hessian of an objective function with respect to both mode transition times and parameters. The objective function is a measure of the error between a measured trajectory and estimated trajectory, calculated using a hybrid model of the system with transition time and parameter estimates.

The estimation technique is demonstrated for a non-linear skid-steered vehicle estimation problem. The algorithms converge to the correct values in simulation, and to values within expected ranges experimentally. The results demonstrate that using a second-order optimization method with an exact Hessian, including the cross-derivative terms, results in convergence in significantly fewer iterations than when first-order or approximate second-order methods are used, and provide sufficient conditions for optimality. Additionally, graceful degradation of estimation performance as a function of measurement noise is demonstrated using Monte Carlo simulation.

The estimation method presented can be applied to a range of hybrid, nonlinear dynamic systems. In addition to calibration and identification applications, information gained in this way is useful in planning and control. Selection of subsequent control strategy, for example, may be dependent on terrain parameters. Similar derivations with respect to switching times [1]–[3] and parameters [4] independently can be found in previous work, however the derivations presented here are based on introductory calculus techniques, and the proof extends to cross-derivative terms in the Hessian.

Related work in hybrid parameter estimation is discussed in Section I-A. The skid-steered vehicle, used as a motivating example and experimental platform, is introduced in Section I-B. The problem formulation and notation are presented in Section II. Sections III and IV present the derivations of the first- and second- order optimality conditions with respect to both transition times and parameters. The estimation method is verified using a skid-steered vehicle as an example in Section V.

A. Related Work

The mathematical results presented are based on previous work in estimation of switching times and parameters. Switching time estimation using optimal control techniques has been presented in several previous publications [1]–[3]. In particular, the first-and second-order optimality conditions for switching time optimization presented in [1] and [2] are used directly in the derivations in Sections III-A and IV-A. Parameter estimation using adjoint methods similar to the results derived here are presented in [4] in order to calculate the second-order derivatives with respect to parameters, using multiplier methods and in the case of continuous systems. The results derived in Sections III-B and IV-B are similar, but the proof relies only on introductory calculus techniques. As a consequence, the results generalize to the cross derivative terms which we show to be critical in achieving quadratic convergence.

The authors are with the Department of Mechanical Engineering, Northwestern University, Evanston, IL, 60208 USA (e-mail: LaurenMiller@U.Northwestern.edu, T-Murphey@Northwestern.Edu)

A numerical optimization approach to a similar estimation scenario for the case of impulsive systems was derived in [5], where unknown parameters are estimated using quasi-Newton methods. The results we present, however, provide an efficient way of calculating the terms necessary for exact second-order optimization methods and the sufficient conditions for optimality. In [6] a similar hybrid parameter estimation problem is solved, but in the context of periodic orbit data, using a trust-region based optimization method relying on first and second derivatives obtained via automatic differentiation and finite differencing, respectively.

A multi-pass estimation technique using hidden Markov models and a nonlinear least squares is used in [7] to estimate contact states and object properties for manipulation tasks. We propose an approach capable of solving the same class of problems while relying on straightforward optimization techniques, avoiding the combinatorial complexity MCMC methods necessarily involve.

The derivations of the optimality conditions and the skid-steered vehicle model used in this work can also be found in previous work by the authors [8]. The results presented in [8] are expanded upon here, including the effect of measurement noise, and a larger set of simulated and experimental examples.

B. Motivating Example: Skid-Steered Vehicle

The motivating example used in this paper is a skid-steered vehicle driving on non-deformable surfaces with GPS tracking. Skid-steered vehicles present a challenge from modeling, trajectory-tracking, and control design perspectives. A skid-steered vehicle can turn only by skidding laterally, which introduces dynamics that are distinct from forward rolling-without-slipping and are dependent on typically uncertain environmental factors, such as frictional forces. Localization and planning for skid-steered vehicles operating on uncertain terrain often require either sensor fusion and filtering techniques for localization [9]–[11], robust control techniques [12], [13], or on-line estimation of the vehicle state and environmental parameters [14], [15], which will be addressed in this paper.

A number of friction models have been established to represent tire-ground interaction for vehicles driving on non-deformable terrain [16]–[19]. More sophisticated friction models typically involve larger numbers of parameters, 16-31 in the case of Pacejka's Magic Tire formula [18]. These parameters are typically identified with a large number of steady-state, highly controlled laboratory experiments, which makes estimating a high number of parameters possible.

With the intention of performing efficient online terrain estimation with limited sensing, such as sparse GPS data, the skid-steered vehicle in this paper is modeled as a hybrid system, with modes dependent on whether or not the wheels are slipping with respect to the ground, using a simple stick-slip viscous friction model. While a stick-slip friction model does not characterize frictional forces at the tire-road interface level as precisely as more sophisticated models, it is nevertheless sufficient to characterize behavior at the vehicle motion level. As will be shown in Section V, the stick-slip model exhibits the same qualitative behavior in simulation as the widely used Pacejka's Magic Tire formula [18] for simple maneuvers, as well as good experimental tracking of the vehicle shown in Fig. 1 given coarsely sampled GPS position measurements. Perhaps most critical in terms of formulating a viable estimation problem, the stick-slip model requires estimation of a single parameter for friction as well as switching times characterizing stick-slip transitions, which becomes a tractable estimation problem for online experiments with sparsely observed, vehicle motion level data while still providing useful terrain information at the motion control level.

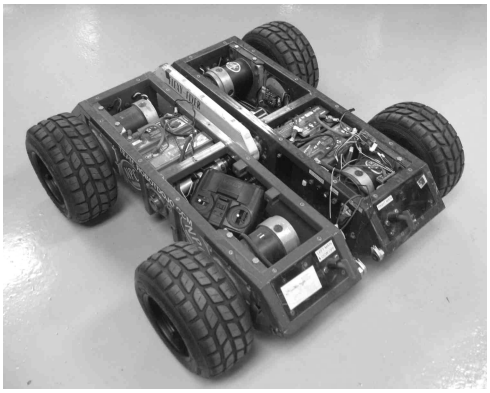

Fig. 1. Skid-Steered vehicle used in experiments

While estimation of a large number of parameters for more sophisticated traction models is not likely a well-conditioned problem for our experimental scenario, it should nevertheless be noted that the estimation method presented in this paper is not specific to this traction model, and although not explored here, friction models with a larger number of parameters may be amenable to the estimation method presented here with higher frequency GPS sampling or additional sensors.

II. Problem formulation and Notation

For the hybrid model used, it is assumed that the number and order of mode transitions are known in advance. This is a reasonable assumption if the driver inputs to the vehicle are known, although model and environmental parameter uncertainty typically result in variations in the transition times and trajectory. The problem is therefore, given the control inputs, system model, and potentially coarse positional tracking data, to have a method of estimating transition times and parameters in order to represent the continuous path of the vehicle for localization and planning of future control strategy.

The hybrid system model and notation used throughout this paper follow [2]. As in [2], slot derivative notation is used throughout; i.e. $D_n f(arg_1, arg_2, ...)$ is the derivative of the function $f(\cdot)$ with respect to the argument at position n. $D_{arg}(...)$ is the derivative with respect to arg . The $\circ$ operator is used to represent linear mappings, for example $M \circ v = M \cdot v$, and $M \circ (v, u) = v^T[M]u$.

A general hybrid system with n dimensions, N transitions, and M parameters of interest can be described by a sequence

of dynamic equations of the form

$$\dot{x} = f_i(x(t), t) \quad \tau_i < t < \tau_{i+1}\ , \quad x(t_0) = x_0 \tag{1}$$

for transition times $\tau = \tau_1, \ldots, \tau_N$ and parameters $p = p_1, \ldots, p_M$, where $\tau_0 = t_0$ is the initial time and $\tau_{N+1} = t_f$ is the final time. Note that throughout this paper, $x(t)$ is written when it should explicitly be $x(\tau_1, \ldots, \tau_N, p_1, \ldots, p_M, t)$, and $f(x(t), t)$ should explicitly be $f(x(t), \tau_1, \ldots, \tau_N, p_1, \ldots, p_M, t)$. Unknown switching times and parameters can be estimated simultaneously by minimizing an objective function of the form

$$J(\tau_1, \ldots, \tau_N, p_1, \ldots, p_M) = \int_{t_0}^{t_f} \ell(x(t), t)dt, \tag{2}$$

where $\ell(x(t), t)$ is an arbitrary incremental cost function, such as $(x(t) - x_m(t))^T (x(t) - x_m(t))$, where $x(t)$ is the estimated trajectory and $x_m(t)$ is the measured trajectory. It is assumed that $\ell(x(t), t)$ does not depend explicitly on the switching times or parameters. It is also assumed that the system trajectory is sampled over a finite time horizon, that the number of switches as well as the mode order is known, and state variables are continuous. Although not addressed here, there are scenarios where the order in which mode changes occur is not known. A method for determining mode order is provided in [1]. Additionally, while in this paper the trajectory $x(t)$ is assumed to be a continuous signal, impulsive optimization techniques [5] would allow the extension of this method to non-continuous state variables.

A. Optimization Methods

Sequential Quadratic Programming (SQP) is used as an optimization framework for comparing first, and exact and approximate second-order, convergence. SQP involves solving a quadratic program at each iteration, subject to a set of constraints on the order of the switching times. Three choices of the quadratic term were compared. Setting the quadratic term equal to zero is equivalent to a first-order, steepest descent algorithm, resulting in linear convergence. Quadratic convergence is obtained using the exact Hessian, which involves the cross-derivative terms between the switching times and parameters, i.e.

$$\text{exact Hessian} : \begin{pmatrix} D_\tau^2 J & D_p D_\tau J \\ D_\tau D_p J & D_p^2 J \end{pmatrix}, \tag{3}$$

derived in Section IV. The effects of using an approximate, block-diagonal Hessian, not including the cross-derivative terms, as the quadratic term

$$\text{block-diagonal Hessian} : \begin{pmatrix} D_\tau^2 J & 0 \\ 0 & D_p^2 J \end{pmatrix} \tag{4}$$

are also examined. Both SQP and steepest descent algorithms are well-established. For more information, see [20].

For the skid-steered vehicle example in Section V, a combination of steepest descent and SQP was used. While second-order optimization methods (SQP) result in fast convergence, they are only viable in locally convex regions of the cost function. It is therefore typically necessary to iterate initially using steepest descent, switching to a second-order method when the Hessian is determined to be positive definite.

III. First-Order Optimality Conditions

$DJ(\cdot)$ involves the derivatives of $J(\cdot)$ with respect to switching times and parameters. $DJ(\cdot)$ is the $N + M$ length vector

$$DJ(\cdot) = (D_{\tau_1} J, \ldots, D_{\tau_N} J, D_{p_1} J, \ldots, D_{p_M} J). \tag{5}$$

The calculations of $D_{\tau_i} J$ and $D_{p_i} J$ follow.

A. Calculating $D_{\tau_i} J(\cdot)$

Complete derivations of first-order partial derivatives of a cost function $J(\cdot)$ with respect to a switching time τ_i are derived in [1], [2]. Those results are presented here, as they are used directly in the second-order and parameter derivations.

Lemma 1: The first partial derivative of the cost function in Eq. (2) with respect to each switching time $\tau_i \ \forall \ i = 1, ..., N$ is calculated as

$$D_{\tau_i} J(\cdot) = \psi(\tau_i) \circ X^i, \tag{6}$$

where $\psi(t)$ is the n-length first-order adjoint found by solving the following backwards differential equation:

$$\dot{\psi}(t) = -D\ell(x(t)) - \psi(t) \circ D_1 f(x(t), t), \quad \psi(t_f) = 0. \tag{7}$$

$X^i \in \mathbb{R}^n$ is defined as shown below for compactness, following [2].

$$X^i = f_{i-1}(x(\tau_i), \tau_i) - f_i(x(\tau_i), \tau_i) \tag{8}$$

A proof of Lemma 1 can be found in [2].

B. Calculating $D_{p_i} J(\cdot)$

Lemma 2: The first partial derivative of the objective function with respect to a parameter p_i is calculated as

$$D_{p_i} J(\cdot) = \int_{t_0}^{t_f} \psi(t) \circ D_{p_i} f(x(t), t)dt, \tag{9}$$

where $\psi(t)$ is the same adjoint used in Lemma 1, calculated using Eq. (7). Note that Eq. (9) is simply an inner product.

Proof: The cost function from Eq. (2) is differentiated with respect to a parameter p_i, applying the chain rule as follows:

$$D_{p_i} J(\cdot) = \int_{t_0}^{t_f} D\ell(x(s)) \circ D_{p_i} x(s)ds.$$

This expression depends on the partial derivative of $x(t)$ with respect to a parameter p_i. $D_{p_i} x(s)$ is obtained by writing segments of the trajectory in integral form,

$$x(t_0) = x_0 \qquad x_k(t) = x_{k-1}(\tau_k) + \int_{\tau_k}^{t} f_k(x_k(s), s)ds,$$

and taking partial derivative of each segment $x_k(t)$ of the trajectory to obtain a linear differential equation for $D_{p_i} x_k(t)$.

$$\begin{aligned} D_{p_i} x_k(t) = & D_{p_i} x_{k-1}(\tau_k) + \int_{t_0}^{t} D_1 f_k(x(s), s) \circ D_{p_i} x_k(s) \\ & + D_{p_i} f_k(x(s), s)ds \end{aligned}$$

Using the fundamental theorem of calculus, the above equation can be expressed in differential form:

$$\begin{aligned} D_{p_i}x_k(\tau_k) =& D_{p_i}x_{k-1}(\tau_k), \\ \frac{\partial}{\partial t}D_{p_i}x_k(t) =& D_1 f_k(x(t),t)\circ D_{p_i}x_k(t) + D_{p_i}f_k(x(t),t). \end{aligned}$$

The equation above is of the form $\dot{z}(t) = A(t)z(t) + B(t)$, which has the solution

$$\begin{aligned} D_{p_i}x_k(t) =& \Phi(t,\tau_k)D_{p_i}x_{k-1}(\tau_k) \\ &+ \int_{\tau_k}^{t} \Phi(t,\sigma)\circ D_{p_i}f_k(x(\sigma),\sigma)d\sigma, \end{aligned}$$

where the state transition matrix $\Phi(t,\tau_k)$ is the solution to $\dot{z}(t) = D_1 f_k(x(t),t)\circ z(t)$ [2]. For more information on the state transition matrix, see [21]. Because the initial condition $D_{p_i}x_{k-1}(\tau_k)$ depends recursively on the same expression for the previous segment of the trajectory and $D_{p_i}x(t_0) = 0$, $D_{p_i}x(t)$ can be expressed as a continuous trajectory:

$$D_{p_i}x(t) = \int_{t_0}^{t} \Phi(t,\sigma)\circ D_{p_i}f(x(\sigma),\sigma)d\sigma. \tag{10}$$

Plugging the expression for $D_{p_i}x(t)$ from Eq. (10) into the expression for $D_{p_i}J$ yields

$$D_{p_i}J(\cdot) = \int_{t_0}^{t_f} D\ell(x(s)) \int_{t_0}^{s} \Phi(s,\sigma)\circ D_{p_i}f(x(\sigma),\sigma)d\sigma ds.$$

Switching the order of integration and pulling $D_{p_i}f(x(\sigma),\sigma)$ outside the inner integral, the following equation is obtained:

$$\begin{aligned} D_{p_i}J(\cdot) = \int_{t_0}^{t_f} \left(\int_{\sigma}^{t_f} D\ell(x(s))\circ\Phi(s,\sigma)ds \right) \\ \circ D_{p_i}f(x(\sigma),\sigma)d\sigma. \end{aligned}$$

The operator $\psi(t)$ can thus be defined as the inner integral $\int_t^{t_f} D\ell(x(s))\circ\Phi(s,t)ds$, which when differentiated with respect to t results in Eq. (7), the same backwards adjoint equation as used in the derivative with respect to a switching time. ∎

A single integration of $\psi(t)$ is used to calculate the values of the gradient with respect to all switching times, over the entire time horizon with respect to all parameters, and can be calculated and stored once per iteration. Additionally, note that the proof is only taking advantage of the chain rule.

IV. Second-Order Optimality Conditions

The Hessian with respect to switching times and parameters, $D_\tau^2 J(\cdot)$, is an $(N+M)\times(N+M)$ matrix, shown in block form in Eq. (3).

A. Calculating $D_{\tau_j}D_{\tau_i}J(\cdot)$

The second derivative of the cost function with respect to switching times τ are derived in [1], [2]. The notation once again follows that of [2] for compactness.

Theorem 1: The second derivative of the cost function with respect to two switching times τ_i and τ_j is calculated as follows:

$$\begin{aligned} D_{\tau_j}D_{\tau_i}J(\cdot) =& -D\ell(x(\tau_i))\circ X^i\delta_i^j + \psi(\tau_i)\circ X^{i,j} + \\ & \Omega(\tau_i)\circ(\Phi(\tau_i,\tau_j)\circ X^j, X^i), \end{aligned} \tag{11}$$

where δ is the Kronecker delta. This equation involves the $n\times n$ second-order adjoint $\Omega(t)$, which is found by solving the following backwards differential equation:

$$\begin{aligned} \Omega(t_f) =& 0_{(n\times n)} \\ \dot{\Omega}(t) =& -D^2\ell(x(t)) - \psi(t)\circ D_1^2 f(x(t),t) - \\ & [D_1 f(x(t),t)]^T\circ\Omega(t) - \Omega(t)\circ D_1 f(x(t),t). \end{aligned} \tag{12}$$

The terms in $X^{i,j}$ are defined as

$$X^{i,j} = \begin{cases} D_1 f_i(x(\tau_i),\tau_i)\circ f_i(x(\tau_i),\tau_i) \\ +D_1 f_{i-1}(x(\tau_i),\tau_i)\circ f_{i-1}(x(\tau_i),\tau_i) \\ -2D_1 f_i(x(\tau_i),\tau_i)\circ f_{i-1}(x(\tau_i),\tau_i) \\ +D_2 f_{i-1}(x(\tau_i),\tau_i) - D_2 f_i(x(\tau_i),\tau_i) & i=j \\ \\ [D_1 f_{i-1}(x(\tau_i),\tau_j) - D_1 f_i(x(\tau_i),\tau_i)] \\ \circ\Phi(\tau_i,\tau j)\circ X^j & i>j. \end{cases} \tag{13}$$

A proof of Theorem 1 can be found in [2].

B. Calculating $D_{p_j}D_{p_i}J(\cdot)$

Theorem 2: The derivative of $J(\cdot)$ with respect to two parameters p_i and p_j can be calculated as follows:

$$\begin{aligned} D_{p_j}D_{p_i}J(\cdot) = \int_{t_0}^{t_f} & D_{p_i}f(x(t),t)^T\circ\Omega^{p_j}(t) \\ & + \psi(t)\circ[D_{p_j}D_{p_i}f(x(t),t) \\ & + D_1 D_{p_i}f(x(t),t)\circ D_{p_j}x(t)]dt, \end{aligned} \tag{14}$$

where $\Omega^{p_j}(t)$ is an n-length vector second-order adjoint equation, unique to each parameter, calculated by solving the differential equation

$$\begin{aligned} \Omega^{p_j}(t_f) =& 0_{(n)} \\ \dot{\Omega}^{p_j}(t) =& -D^2\ell(x(t),t)\circ D_{p_j}x(t) - \\ & [D_1 f(x(t),t)]^T\circ\Omega^{p_j}(t) - \\ & \psi(t)\circ[D_1^2 f(x(t),t)\circ D_{p_j}x(t) + \\ & D_{p_j}D_1 f(x(t),t)]. \end{aligned} \tag{15}$$

Proof: Differentiating $D_{p_i}J(\cdot)$ with respect to the parameter p_j yields

$$\begin{aligned} D_{p_j}D_{p_i}J(\cdot) = \int_{t_0}^{t_f} & \frac{\partial}{\partial p_j}[\psi(t)]\circ D_{p_i}f(x(t),t) \\ & + \psi(t)\circ\frac{\partial}{\partial p_j}[D_{p_i}f(x(t),t)]\,dt \end{aligned}$$

A second-order adjoint, $\Omega^{p_j}(t) = \frac{\partial}{\partial p_j}[\psi(t)]$, is defined for the second derivative with respect to the parameters. $\Omega^{p_j}(t)$ is obtained by differentiating the expression for first-order adjoint, $\dot{\psi}(t)$, with respect to a parameter p_j (the initial condition remains zero), and integrating backwards in time as in the first-order derivation.

$\frac{\partial}{\partial p_j}[D_{p_i}f(x(t),t)]$ is calculated by differentiating $D_{p_i}f(x(t),t)$ with respect to a parameter p_j:

$$\begin{aligned} \frac{\partial}{\partial p_j}[D_{p_i}f(x(t),t)] = \int_{t_0}^{t_f} & D_{p_j}D_{p_i}f(x(s),s) \\ & + D_1 D_{p_i}f(x(s),s)\circ D_{p_j}x(s)ds. \end{aligned}$$

At this point, $\Omega^{p_j}(t)$ and $D_{p_j}D_{p_i}J(\cdot)$ can be substituted into the expression above to obtain Eq. (14). ■

As mentioned, the same expression for second-order derivatives with respect to parameters are derived in [4] using multiplier methods, however the proof presented above is more concise and the methods used generalize clearly to the results proven in Section IV-C.

C. Calculating $D_{\tau_i}D_{p_i}J(\cdot)$

In order to simultaneously optimize over switching times and parameters, the complete Hessian also involves the derivative with respect to both a switching time and a parameter.

Theorem 3: The derivative of the cost function with respect to both a switching time τ_i and a parameter p_j is calculated as follows,

$$D_{\tau_i}D_{p_j}J(\cdot) = \psi(\tau_i)\circ X^{\tau,p} + [X^i]^T \circ \Omega^{p_j}(\tau_i) \tag{16}$$

where $\psi(\tau_i)$, X^i, $\Omega^{p_j}(\tau_i)$, are defined by Eqs. (7), (8), and (15), respectively. $X^{\tau,p}$ is defined as

$$\begin{aligned} X^{\tau,p} = &[D_1 f_{i-1}(x(\tau_i),\tau_i) - D_1 f_i(x(\tau_i),\tau_i)]\circ D_p x(\tau) \\ &+ [D_p f_{i-1}(x(\tau_i),\tau_i) - D_p f_i(x(\tau_i),\tau_i)]\,. \end{aligned} \tag{17}$$

Proof: Differentiating $D_{\tau_i}J(\cdot)$ in Eq. (6) with respect to the parameter p_j yields

$$D_{p_j}D_{\tau_i}J(\cdot) = \psi(\tau_i)\circ X^{\tau,p} + \frac{\partial}{\partial p_j}\psi(\tau_i)\circ X^i.$$

$X^{\tau,p}$ represents $\frac{\partial}{\partial p_j}X^i$, the derivative of the initial conditions X^i with respect to a parameter. Equation (17) is obtained by differentiating and applying the chain rule to Eq. (8).

The second term involves $\frac{\partial}{\partial p_j}\psi(\tau_i)$, which is the same second-order adjoint $\Omega^{p_j}(t)$ derived previously, evaluated at the switching time τ_i. ■

The adjoint equations (7) and (15), derived in the context of hybrid systems, are derived in [4] for continuous systems using multiplier methods. The derivation of the second order derivative with respect to parameters presented in this paper, in addition to applying to hybrid scenarios, is generalized to the cross-derivative terms between switching times and parameters, which is shown to be critical for fast convergence.

V. Example: The Skid-Steered Vehicle

In this section, the proposed estimation algorithm is applied to a sampled skid-steered vehicle trajectory, for both simulated and experimental data. The vehicle model is made up of four wheels connected to a rigid body. The vehicle turns if the applied differential torque is large enough to cause slipping between the tires and the ground, resulting in skidding. The wheel-ground interaction is modeled as stick-slip linear viscous friction, and both the experiment and simulation for the skid-steered vehicle assume non-deformable terrain. The coefficient of friction for the skid-steered vehicle example is treated as an unknown parameter.

Only the modes in which all wheels are slipping (turning) or all wheels are sticking (driving straight) are considered. While modes in which the front wheels are sticking and rear wheels are slipping, or vice versa, are potential modes for this system, these modes were not observed experimentally using the input torque profile. Additionally, mode sequence estimation presented in [1] determined that switching from all wheels sticking to all wheels slipping was the expected mode order for similar torque profiles.

A diagram of the skid-steered vehicle model used is shown in Fig. 2. The vehicle configuration is $x = (X, \dot{X}, Y, \dot{Y}, \theta, \dot{\theta})$, where X and Y are Cartesian coordinates with respect to the vehicle center of mass, and θ represents the heading of the vehicle in the global frame. The equations of motion are adopted from [1] and are shown below for a vehicle that turns once, switching from sticking to slipping, and back to sticking.

$$\text{In stick mode: } \begin{cases} \ddot{X} = \frac{(F_1+F_2+F_3+F_4)cos\theta(t) - c_1\dot{X}(t)}{(m_b+4m_w)} \\ \ddot{Y} = \frac{(F_1+F_2+F_3+F_4)sin\theta(t) - c_1\dot{Y}(t)}{(m_b+4m_w)} \\ \ddot{\theta} = 0 \end{cases}$$

$$\text{In slip mode: } \begin{cases} \ddot{X} = \frac{(F_1+F_2+F_3+F_4)cos\theta(t) - c_2\dot{X}(t)}{(m_b+4m_w)} + \\ g\mu_k sin\theta(t)\left(-sin\theta(t)\dot{X}(t) + cos\theta(t)\dot{Y}(t)\right) \\ \ddot{Y} = \frac{(F_1+F_2+F_3+F_4)sin\theta(t) - c_2\dot{Y}(t)}{(m_b+4m_w)} - \\ g\mu_k cos\theta(t)\left(-sin\theta(t)\dot{X}(t) + cos\theta(t)\dot{Y}(t)\right) \\ \ddot{\theta} = \frac{12b(F_1-F_2-F_3+F_4) - 12a^2 g(m_b+4m_w)\mu_k\dot{\theta}(t)}{4m_w(12a^2+12b^2)+m_b(B_l^2+B_w^2)} \end{cases}$$

$$\dot{x} = f(x,t) = \begin{cases} \text{sticking} & 0 \le t < \tau_1 \\ \text{slipping} & \tau_1 \le t < \tau_2 \\ \text{sticking} & \tau_2 \le t < 1 \end{cases} \tag{18}$$

In Eq. (18), F_1, F_2, F_3, and F_4 are the transformed wheel torques sent to each of the wheels. The estimated coefficient of friction is μ_k, and all other model parameters for the vehicle used experimentally, shown in Fig. 1, are known: g is the gravitational constant, $m_w = 2.5$ kg and $m_b = 70$ kg are the masses of the wheel and car body, $B_l = 0.89$ m and $B_w = 0.55$ m are the length and width of the vehicle body, $a = 0.25$ m and $b = 0.23$ m are the distances from the wheels to the center of mass in each dimension, c_1 and c_2 are system identified internal damping coefficients, set to 0.72 and 0.92 respectively. The incremental cost function used in the simulations and experiments was $\ell(x(t),t) = \frac{1}{2}\left(x(t) - x_m(t)\right)^T\left(x(t) - x_m(t)\right)$.

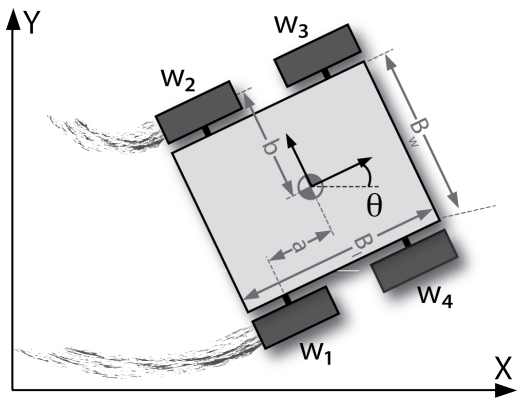

Fig. 2. Skid-Steered vehicle model used in simulation

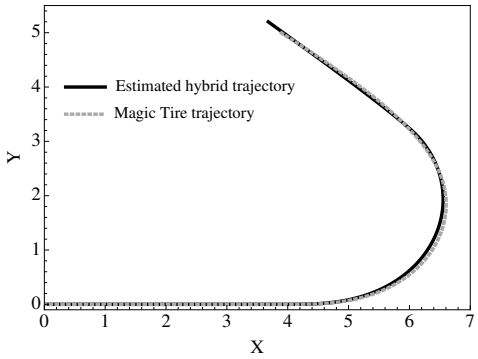

Fig. 3. Reference trajectory generated using Magic Tire formula (dashed gray) and optimized hybrid trajectory generated using optimal friction coefficient and switching times (solid black line).

A. Simulation

The estimation method requires a model of the system, commanded control inputs, and a measured trajectory for optimal estimation. In this section, the measured vehicle trajectory was simulated using two different traction models in Mathematica– Pacejka's Magic Tire formula [18] and the stick-slip friction model in Eq. (18). In both cases the hybrid stick-slip model is used for forward simulation in the estimation algorithm.

1) Estimation of friction coefficient and switching times for a trajectory generated using the Magic Tire formula: Rather than assuming that the forces at the wheels in Eq. (18) change instantaneously (assuming stick-slip), the forces at each wheel in this example are calculated using the Magic Tire Formula, with model parameters taken from [18]. In this case, the wheel angular velocities are assumed to switch from all positive values, to a differential, and back. The version of the Magic Tire Formula implemented involves 16 different coefficients; numerically calculating the Hessian of the objective function with respect to the 16 Magic Tire parameters at the optimal values, however, yields an ill-conditioned matrix. In particular, the first singular value is 7, while the next largest one is 0.7 and all the rest are close to zero. This motivates use of the stick-slip model for estimation, involving one unknown parameter and switching times.

Using the hybrid stick-slip model for estimation, the algorithm converged to reasonable values, obtaining necessary and sufficient conditions for optimality, and produced a trajectory which tracked the Magic Tire reference well. Figure 3 shows the trajectory generated using the Magic Tire formula as a dashed gray curve, and the optimized stick-slip trajectory in solid black. The wheel angular velocity inputs to the magic tire model were programmed to switch at 5 and 10 seconds; the optimal switching times obtained using the hybrid stick-slip model are 5 and 11.7 seconds with a coefficient of friction of 0.676. The coefficient of friction estimate is within reasonable bounds for tires on asphalt [22]. The difference in the second switching time is likely a result of the difference between the stick-slip model, which assumes the vehicle instantaneously regains traction, and the Magic Tire model, which results in a transient turning period after the angular velocity inputs switch; in the hybrid model, this transient turning results in an optimal trajectory with a delayed second stick-slip transition time.

2) Estimation of friction coefficient and switching times using a stick-slip friction model: Using the equations of motion in Eq. 18 the simulated torque inputs were programmed to transition from F_1=F_2=F_3=F_4=15N, to F_1=F_4=27N, F_2=F_3=0N, then back to F_1=F_2=F_3=F_4=15N. The simulated measured trajectory was generated using ($\mu_k = 0.7$, $\tau_1 = 6$s, $\tau_2 = 10$s). The estimation algorithm was initialized to $(\mu = 0.8, \tau_1 = 5\text{s}, \tau_2 = 9)\text{s}$.

Figure 4 shows logarithmic plots of the norm of the gradient at each iteration using three different choices of quadratic model for the optimization to obtain the transition-time and parameter estimates from simulated data: steepest descent using only first-order derivative information, SQP using a block-diagonal Hessian and SQP using the exact Hessian in simulation. Using steepest descent, the algorithm converged to within a tolerance of 10^{-7} on the norm of the gradient after about 1000 iterations. Using SQP with the exact Hessian, the correct values were determined after only 12 iterations. When SQP was performed using a block diagonal approximation of the Hessian, the convergence does not exhibit the fast quadratic performance observed using the exact Hessian including the cross-derivative terms.

3) Effect of measurement noise on estimation error: A preliminary study of the effect of measurement noise on the error between the measured and simulated trajectory for each switching time and parameter was conducted. Simulated trajectories were generated using the same switching times and parameters. The vehicle position was then sampled at one second intervals, interpolated and low-pass filtered to simulate coarsely sampled GPS measurements. Interpolation is necessary as the algorithm assumes continuous state variables, and filtering accounts for some process noise and improves robustness. Random Gaussian noise was added to each sampled data point, with a mean of zero and variance between 0 and 0.25 m. As shown in Fig. 5, normalized error between values used to generate the sampled trajectory and

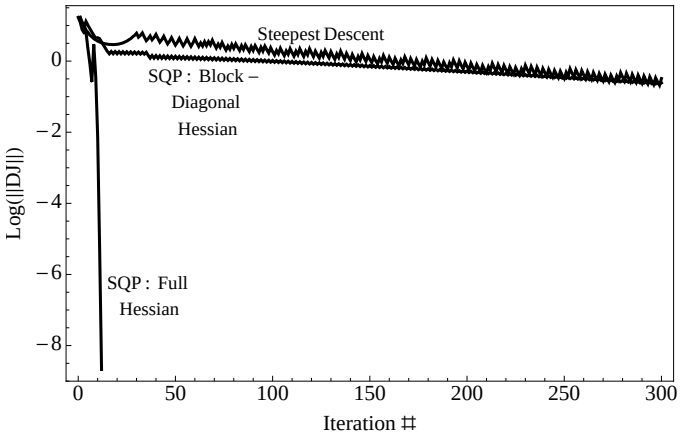

Fig. 4. The logarithm of the norm of the gradient of the cost function, with respect to both switching times and parameters, is shown at every iteration for the three algorithms used; steepest descent and SQP using both exact (SQP: Full Hessian) and approximate (SQP: Block-Diagonal Hessian) Hessians.

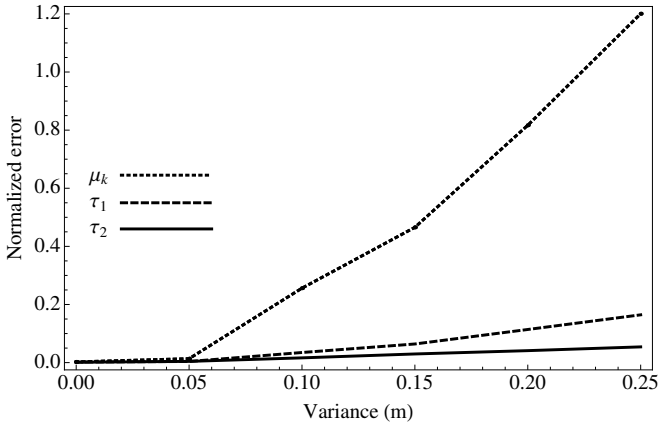

Fig. 5. Normalized error from the estimated switching time and parameter values to the true values for different levels of variance in Gaussian measurement noise

estimated switching times and parameter values increases with the variance of injected Gaussian noise. The error is zero for zero noise, and the performance shows graceful degradation as the noise variance increases up to 0.25 m. The parameter estimate is most sensitive to higher levels of noise. Based on the mode order used in this example, with data sampled at 1 Hz over a 15 second time interval, there are effectively only four measurements which affect the estimate of the friction coefficient (the coefficient only enters the dynamics during slip mode between 5-9s); it is not surprising that this results in increased noise sensitivity with respect to the friction coefficient.

B. Experiment

The estimation method was implemented experimentally using the skid-steered vehicle shown in Fig. 1 on asphalt. Measurements were made using an onboard GPS at 1 Hz, and the data was low-pass filtered and interpolated. Figure 6 shows the raw GPS data collected during the experiment, as well as the interpolated and filtered curves used as the continuous measurement trajectory $x_m(t)$ in the optimization algorithm, plotted as dashed gray lines for five experimental trials. The torque inputs for Trials 1-3 were programmed to transition from F_1=F_2=F_3=F_4=12N, to F_1=F_4=27N, F_2=F_3=0N, then back to F_1=F_2=F_3=F_4=12N; inputs for trials 4 and 5 were programmed to transition from F_1=F_2=F_3=F_4=15N, to F_1=F_4=27, F_2=F_3=0N, then back to F_1=F_2=F_3=F_4=15N. The trajectories that correspond to the optimal estimate of the values of the switching times and parameters for both trials are plotted in black. For all five trials, the estimates were initialized to $\tau = (5, 10)$s, $\mu = 0.8$; the trajectory simulated using the initial values are plotted in solid gray for each trial. Transition times and parameters that correspond to an optimal estimation, according to the interpolation method and objective function chosen, are shown in Fig. 6 for each trial.

All trials converged to within a tolerance of $||DJ|| < 10^{-7}$ on the norm of the gradient in fewer than 15 iterations. The initial conditions were chosen based on approximate knowledge of terrain and the known control inputs for the vehicle. Because control inputs to the vehicle are known (as well as mode order), transition times are typically approximately known, based on when a differential is commanded to the wheels. Although the algorithm is initialized to values that are relatively close to the correct values, choosing initial values further from the optimal estimate would generally lead to the same estimate.

The experiment was carried out on an asphalt surface; imperfections in the surface as well as the possibility of the presence of other material, e.g. sand or dirt, introduce variability in the transition times and friction coefficient. Unmodeled mechanical and electrical factors such as battery discharge also contribute to uncertainty. Expected values for the coefficient of friction of rubber on asphalt range from 0.6-0.85 [22]. All estimated trajectories qualitatively follow the interpolation of the data well, the estimated coefficient for trials 1-4 are within the range of expected values, and the values are very similar for trials 1, 2, and 4. In trial 5 a parameter value outside the expected range is calculated. There are several possible reasons for this difference. Given that experiments were carried out in an outdoor environment it is possible that there was a variation in the surface properties in the region traversed during trial 5, or some characteristic of the vehicle itself (e.g. battery discharge) is causing the vehicle to travel and turn marginally more slowly during this trial, resulting in a higher estimated friction coefficient value given the same torque inputs.

VI. Conclusion

An algorithm for estimating both mode transition times and parameters using first- and second-order optimization methods for a hybrid system operating in uncertain conditions is presented. The main contributions are analytical derivations of the Hessian and gradient with respect to mode transition times and parameters. The results rely only on standard calculus techniques that generalize to hybrid systems and cross-derivative terms between the switching times and parameters. The results demonstrate the ability of the optimization-based estimation algorithm to perform well given coarsely sampled experimental data. Simulation results demonstrate dramatic increase in convergence rates using second-order methods within the SQP framework using the exact Hessian.

Several potentially limiting assumptions were made in the formulation of the estimation method presented. It is assumed that mode order is known, and that the state evolves continuously. While reasonable for the examples provided, mode order is not always predictable, and there are many systems which experience discontinuities in the state, such as impacting systems. Generalization of the approach to include optimization over mode order as well as impulse magnitude will be included in future work. The optimization-based estimation technique also requires that the system trajectory is sampled over a finite time horizon. Further analysis is planned to characterize how the length of this time horizon affects the robustness of the optimization problem; shorter time intervals are likely desirable from a computational perspective, however shorter time intervals may result in a less well-posed optimization problem.

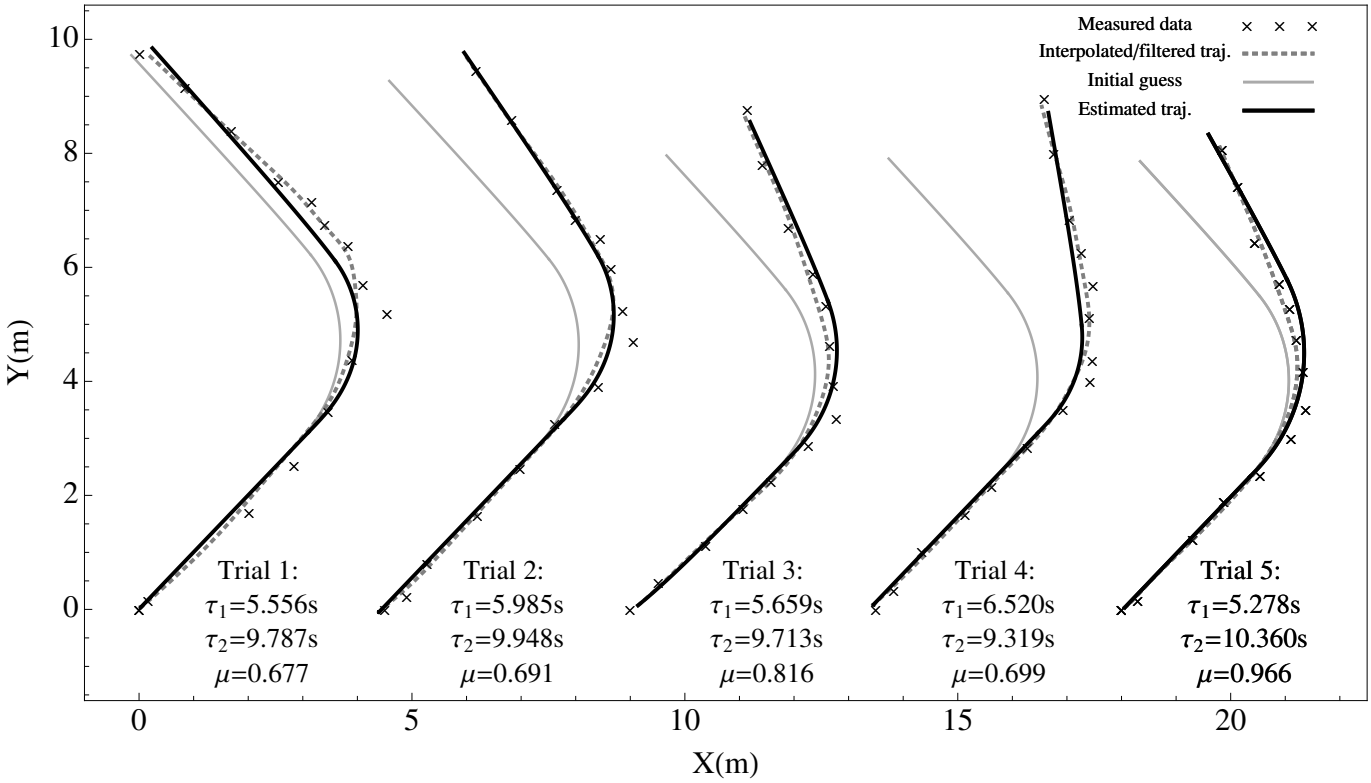

Fig. 6. Measured data and trajectory generated using the optimal estimates of transition times and parameters for five trials of the skid steered vehicle driving on an asphalt surface. Trajectories are shifted along the X axis for visualization.

ACKNOWLEDGMENT

This material is based upon work partially supported by the National Science Foundation under Grant IIS-0917837. Any opinions, findings, and conclusions or recommendations expressed in this material are those of the authors and do not necessarily reflect the views of the National Science Foundation.

REFERENCES

[1] T. Caldwell and T. Murphey, "Switching mode generation and optimal estimation with application to skid-steering," *Automatica*, vol. 47, no. 1, pp. 50 – 64, 2011.

[2] E. Johnson and T. Murphey, "Second-order switching time optimization for nonlinear time-varying dynamic systems," *IEEE Transactions on Automatic Control*, vol. 56, no. 8, pp. 1953 –1957, Aug. 2011.

[3] X. Xu and P. Antsaklis, "Optimal control of switched autonomous systems," in *IEEE Int. Conf. on Decision and Control (CDC)*, vol. 4, Dec. 2002, pp. 4401 – 4406.

[4] D. Ozyurt, B. Derya, and P. Barton, "Cheap second order directional derivatives of stiff ODE embedded functionals," *SIAM Journal of Scientific Computing*, vol. 26, no. 5, pp. 1725–1743, May 2005.

[5] A. Damle and L. Pao, "Simultaneous numerical optimization for data association and parameter estimation," in *IEEE Int. Conf. on Decision and Control (CDC)*, Dec. 2011, pp. 7800 –7805.

[6] E. Phipps, R. Casey, and J. Guckenheimer, "Periodic orbits of hybrid systems and parameter estimation via AD," *Automatic Differentiation: Applications, Theory, and Implementations*, pp. 211–223, 2006.

[7] T.J.Debus, P. Dupont, and R. Howe, "Contact state estimation using multiple model estimation and hidden markov models," *International Journal of Robotics Research*, vol. 23, no. 4-5, pp. 399–413, 2004.

[8] L. M. Miller and T. D. Murphey, "Simultaneous optimal parameter and mode transition time estimation," in *IEEE Int. Conf. on Intelligent Robots and Systems (IROS)*, Oct. 2012, pp. 719–724.

[9] G. Anousaki and K. Kyriakopoulos, "A dead-reckoning scheme for skid-steered vehicles in outdoor environments," in *IEEE Int. Conf. on Robotics and Automation (ICRA)*, vol. 1, April 2004, pp. 580 – 585.

[10] L. Ojeda, D. Cruz, G. Reina, and J. Borenstein, "Current-based slippage detection and odometry correction for mobile robots and planetary rovers," *IEEE Transactions on Robotics*, vol. 22, no. 2, pp. 366 –378, April 2006.

[11] S. Zibin, Y. Zweiri, L. Seneviratne, and K. Althoefer, "Non-linear observer for slip estimation of skid-steering vehicles," in *IEEE Int. Conf. on Robotics and Automation (ICRA)*, May 2006, pp. 1499 –1504.

[12] L. Caracciolo, A. de Luca, and S. Iannitti, "Trajectory tracking control of a four-wheel differentially driven mobile robot," in *IEEE Int. Conf. on Robotics and Automation (ICRA)*, vol. 4, 1999, pp. 2632 –2638.

[13] J. Yi, D. Song, J. Zhang, and Z. Goodwin, "Adaptive trajectory tracking control of skid-steered mobile robots," in *IEEE Int. Conf. on Robotics and Automation (ICRA)*, April 2007, pp. 2605 –2610.

[14] K. Iagnemma, K. Shinwoo, H. Shibly, and S. Dubowsky, "Online terrain parameter estimation for wheeled mobile robots with application to planetary rovers," *IEEE Transactions on Robotics*, vol. 20, no. 5, pp. 921 – 927, Oct. 2004.

[15] L. Ray, "Estimation of terrain forces and parameters for rigid-wheeled vehicles," *IEEE Transactions on Robotics*, vol. 25, pp. 717–726, June 2009.

[16] C. Canudas-de-Wit, P. Tsiotras, E. Velenis, M. Basset, and G. Gissinger, "Dynamic friction models for road/tire longitudinal interaction," pp. 189–226, 2003.

[17] E. Velenis, P. Tsiotras, C. Canudas-de-Wit, and M. Sorine, "Dynamic tire friction models for combined longitudinal and lateral vehicle motion," *Vehicle System Dynamics*, vol. 43, no. 1, pp. 3–29, 2005.

[18] E. Bakker, L. Nyborg, and H. Pacejka, "Tyre modelling for use in vehicle dynamics studies," *SAE Technical Paper*, vol. 870421, 1987.

[19] R. Balakrishna and A. Ghosal, "Modeling of slip for wheeled mobile robots," *IEEE Transactions on Robotics and Automation*, vol. 11, no. 1, pp. 126 –132, Feb 1995.

[20] J. Nocedal and S. Wright, *Numerical Optimization*. Springer, 2006.

[21] J. P. Hespanha, *Linear Systems Theory*. Princeton, New Jersey: Princeton Press, Sep. 2009.

[22] J. Stephens, *Kempe's Engineers Year Book*, ser. Kempe's Engineer's Year Book Series. CMP Information, 2001.